J. Kadlec, M. Chadima, L. Lisá, H. Hercman, A. Osintsev, and H. Oberhänsli – Clastic cave deposits in Botovskaya Cave (Eastern Siberia, Russian Federation). *Journal of Cave and Karst Studies,* v. 70, no. 3, p. 142–155.

CLASTIC CAVE DEPOSITS IN BOTOVSKAYA CAVE (EASTERN SIBERIA, RUSSIAN FEDERATION)

Jaroslav Kadlec[1], Martin Chadima[1], Lenka Lisá[1], Helena Hercman[2], Alexandr Osintsev[3], and Hedi Oberhänsli[4]

Abstract: Botovskaya Cave is a typical example of a two-dimensional maze with a total length of explored passages exceeding 60 km, which represents the longest limestone cave system in the Russian Federation. The clastic cave sediments filling the cave passages differ in both mineral and mineral magnetic properties and were deposited under different hydrological conditions. The older portion of the clastic cave fills was derived from overlying sandstones, whereas the properties of younger cave sediments show closer affinity to the soils and weathering products originating on the plateau above the cave. The cave sediments underwent repeated periods of deposition and erosion during the Tertiary (?) and Pleistocene. The last catastrophic erosion event occurred in the cave more than 350 ka based on flowstone dating. Water seeping through the overlying sandstone body causes collapses of sandstone slabs from the cave passage ceilings, forming the youngest portion of the clastic cave fills.

Introduction

It has been demonstrated that the study of the clastic cave deposits can contribute to better understanding of the cave system development as well as to the local hydrological processes. Sedimentological and mineralogical studies together with radiometric or paleomagnetic datings of both clastic and chemogenic deposits have commonly been applied in cave sediment research (e.g., Häuselmann et al., 2007; Kadlec et al., 2001). The mineral magnetic approach has been used only occasionally to understand climatic, hydrological and anthropogenic processes controlling sediment deposition in caves (Ellwood et al., 1996, 2004; Sroubek et al., 2001, 2007). The assemblage of magnetic minerals found in sediments is controlled by the character of the source rocks, weathering, mode and energy of transporting medium, and by depositional as well as post-depositional processes.

The aim of this paper is an examination of Botovskaya Cave deposits using methods operating with magnetic and heavy minerals and with quartz grain exoscopy. Obtained mineral characteristics were used for correlations from the point of view of sediment source and mode of transportation into the cave passages. Radiometric and paleomagnetic datings of the cave carbonate bed allowed us to estimate the age of both depositional and post-depositional processes.

Geographical and Geological Settings

Botovskaya Cave (55° 18′ N, 105° 20′ E) is located on the Angarsko-Lensky Plateau of the southern Siberian Craton about 500 km north of Irkutsk City (Fig. 1). The area reaches altitudes of 1100 m a.s.l., and belongs to the Zhigalovo District of the Irkutsk Area. The plateau is dissected by river valleys up to 400 m deep. Cave entrances lie at a relative elevation of 310 m above the Lena River level, in a valley of the Garevogo Creek, the left tributary of the Boty River, which joins the Lena River. The cave system, dipping gently to the north, has developed in an Early Ordovician limestone formation with a thickness of 6 to 12 m. The limestone bed is underlain by Middle and Late Cambrian sandstone, siltstone, marl and gypsum and overlain by Middle Ordovician sandstone, limestone and argillite (Filippov, 2000).

The cave system developed under confined (artesian karst) settings (Klimchouk, 2000, 2003; Filippov, 2000). The speleogenesis of the Botovskaya Cave system was interpreted by Filippov (2000) and is due to two different processes, (i) corrosion involving meteoric artesian water and (ii) ascending deep circulating artesian water spanning the time period between Late Mesozoic and Early Neogene. The clastic cave deposits fill the bottom portion of the cave passages and are not usually exposed sufficiently for study. The deposits from the cave were preliminarily described by Filippov (2000). Breitenbach (2004) described in detail a recently excavated section of cave sediments (the same section is labeled Section 1 in this paper).

The cave is divided into two parts: the Old World and the New World. All studied sections of cave sediments are situated in the Old World, 200–400 m east of the Central and Medeo entrances (Fig. 2). The key Section 1 and Section 2 are exposed in two test-pits excavated in the sedimentary fill close to survey stations PK0122 and PK042. The smaller Section 3 and Section 4 are located

[1] Institute of Geology AS CR, v.v.i., Rozvojova 269, CZ-165 00 Praha 6, Czech Republic, kadlec@gli.cas.cz
[2] Institute of Geological Sciences, PAN, Warszawa, Poland
[3] Speleoclub Arabica, Irkutsk, Russia
[4] GeoForschungsZentrum Potsdam, Germany

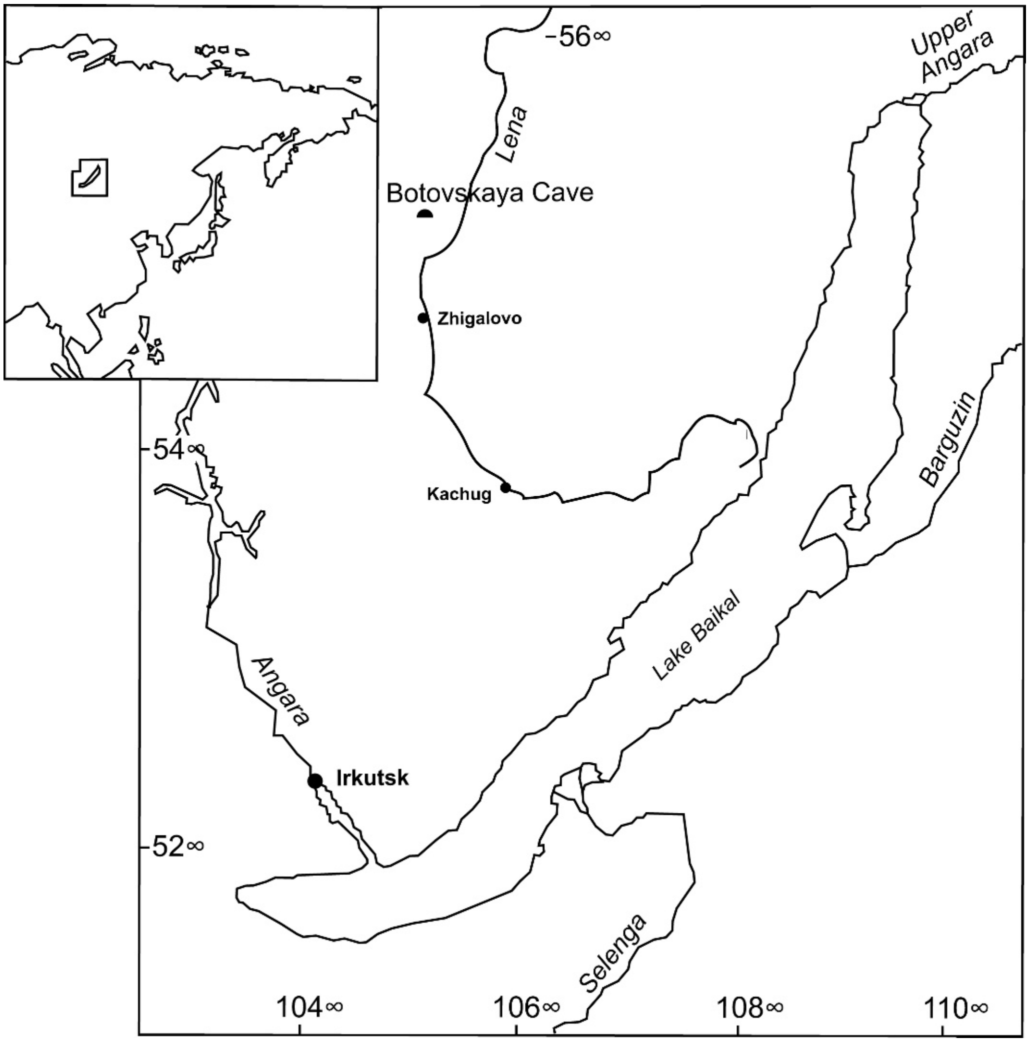

Figure 1. Location of Botovskaya Cave in Eastern Siberia.

close to survey stations PK0186 and PK0342, respectively. A small relic of flowstone bed used for Th/U dating is preserved on the limestone wall W of Section 1 ca 1.7 m above the present passage floor.

Materials and Methods

The studied sections of the cave deposits were documented with special reference to lithology, sedimentary structures and aggradation and erosion event records. Mineral magnetic characteristics such as low field bulk magnetic susceptibility (MS) and anhysteretic remanent magnetization (ARM) together with anisotropy of magnetic susceptibility (AMS) help to find the source of the cave fills and estimate a mode of sediment transport to the cave passages. While MS values are influenced by the concentration of magnetic particles, mineralogy and grain size of the minerals (ferro-, para-, and diamagnetic) in the sediments, ARM is sensitive only to the concentration, mineralogy and grain size of ferromagnetic minerals present in sediments. AMS reflects the preferred orientation of magnetic minerals and can be used for texture interpretation in sedimentary rocks. Magnetic anisotropy can be visualized by an ellipsoid with three perpendicular principal axes ($k_1 \geq k_2 \geq k_3$). The maximum axis (k_1) is denoted as magnetic lineation and the plane perpendicular to minimum axis (k_3) defines a magnetic foliation. The AMS ellipsoid magnitude can be presented as a ratio k_1/k_3, known as the degree of anisotropy, P (Nagata, 1961). The AMS ellipsoid shape can be described by the shape parameter, T (Jelínek, 1981); oblate shapes correspond to $0 < T \leq 1$, prolate shapes correspond to $-1 \leq T < 0$. The degree and shape of the AMS depend on the lithology and compaction imposed on the deposit.

Oriented samples of clastic cave sediments were collected in plastic boxes (volume 6.7 cm^3). For each sample MS and AMS were measured using Agico KLY-4 Kappagridge (alternating field amplitude of 425 A/m and operating frequency of 875 Hz) in the Paleomagnetic Laboratory of the Institute of Geology AS CR, v.v.i. in

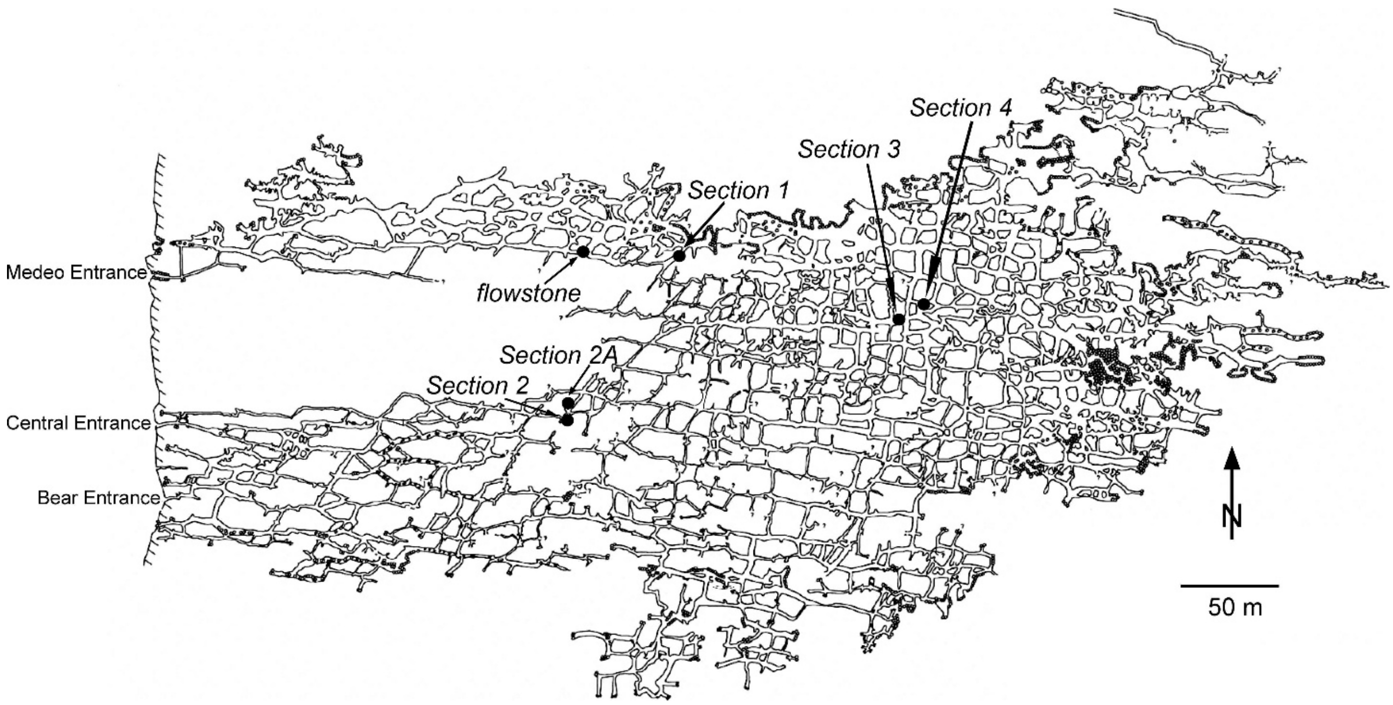

Figure 2. Botovskaya Cave (The Old World) map (adopted from Göbel and Breitenbach, 2003) with indication of studied sections and dated flowstone.

Prague. The ARM was imparted on demagnetized samples (using an Agico AF demagnetizer/magnetizer LDA-3/AMU-1A and measured on an Agico JR-6A spinner magnetometer). Frequency dependent magnetic susceptibility as a proof for the presence of superparamagnetic particles was tested in low- and high-frequency measurements conducted on a Bartington MS2 magnetic susceptibility meter. For the purpose of paleomagnetic polarity measurements three 8 cm^3 samples were cut from the flowstone bed. Samples were thermally demagnetized and measured using a 2G Enterprises superconducting rock magnetometer in the Laboratory for Natural Magnetism ETH Zurich.

The character of quartz grain surfaces indicates transportation and post-depositional history of clastic sediments. Exoscopic observations were performed on quartz grains larger than 0.25 mm separated from either clastic cave deposits or from the Ordovician sandstone bedrock after wet sieving and boiling in HCl. The cleaned grains were stuck on a carbon tape and observed using the BS 340 electron microscope. Heavy minerals were separated after wet sieving from the grain-size fraction of 0.25–0.063 mm using tetrabromethane (density 2.964 g cm^{-3}) and observed in Canadian balsam. At least 300 grains of transparent heavy minerals were determined in each sample.

The flowstone bed used for the paleomagnetic polarity measurements was also dated by the $^{230}Th/^{234}U$ radiometric method. Uranium and thorium were separated from three samples using a standard chemical procedure (Ivanovich and Harmon, 1992). The samples were dissolved in 6 M nitric acid, and uranium and thorium were separated by a chromatographic method using the DOWEX 1 $\times$ 8 ion exchanger. The efficacy of chemical separation was controlled by addition of a $^{228}Th/^{232}U$ spike. Activity measurements (alpha spectrometry) were taken with the OCTETE PC device of the EG&G ORTEC company. Spectral analysis and age calculation were performed using URANOTHOR 2.5. software (Gorka and Hercman, 2002).

DESCRIPTION OF THE CAVE DEPOSITS

SECTION 1

The section is exposed in the excavated test-pit 2.8 m deep (Breitenbach, 2004). A SW face of the test-pit shows dark gray to black, medium-grained sand deposited on the bedrock bottom of the passage (Bed 15 in Fig. 3). The sand layer contains rare laminae of light medium-grained brown sand and sporadic aggregates of SiO_2-cemented sand up to 1 cm large. The overlying gray to yellow brown sand bed contains frequent, up to 2 cm large aggregates of sand cemented with SiO_2 (Bed 14). Deposition continued with brown clayey medium-grained sand with laminae and lenses of light brown sand (Bed 13), light brown, medium-grained sand (Bed 12) and with overlying dark gray clayey medium-grained sand with small lenses to laminae of light fine-grained sand (Bed 11). This bed was partly eroded before the deposition of brown laminated clayey medium-grained sand (Bed 10) with fragments of brown clay on the

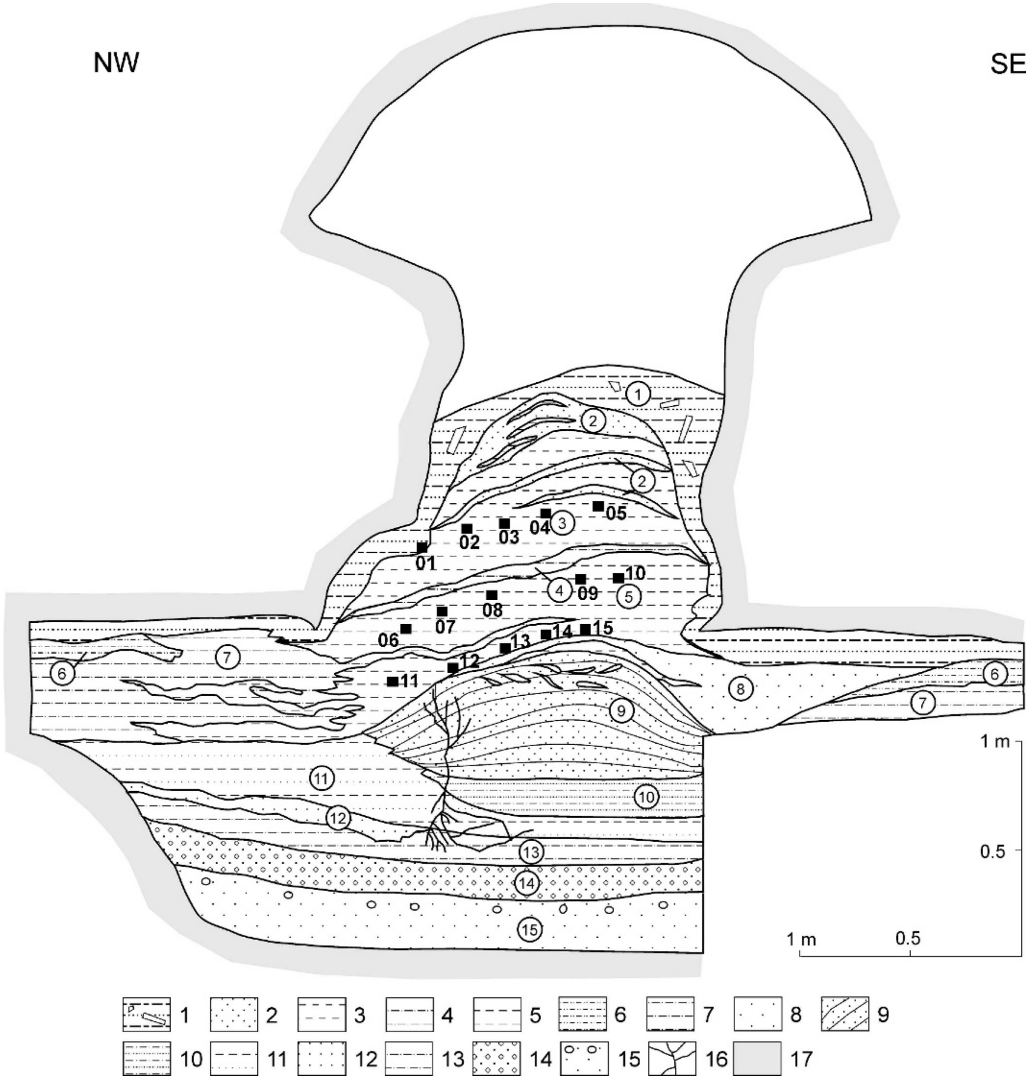

Figure 3. Section 1 — SW face
1 – clay, sporadic angular clasts of sandstone; 2 – sand; 3 – clay; 4 – sandy clay to clayey sand; 5 – clay; 6 – sandy clay; 7 – slightly sandy clay; 8 – sand; 9 – sand, fine-grained; 10 – clayey sand, laminated; 11 – clayey sand; 12 – sand; 13 – clayey sand; 14 – sand with sandy aggregates; 15 – sand; 16 – carbonate cementation along fissures; 17 – bedrock wall; black squares with numbers – collected samples. For more detailed description see text.

erosional top of the bed. The above lying loaf-like bed (Bed 9) is formed by light and dark brown laminae of fine-grained sand 1–15 mm thick with brown clay fragments of up to 2 cm in size at the erosional surfaces and relics of cemented laminae (up to 7 mm thick) in the upper portion of the bed. Beds 9 to 13 were disturbed by fissures filled with carbonate-cemented fine sand. Bed 8 is formed by light brown fine-grained sand with chaotic small lenses or laminae of darker medium-grained sand and rare fragments of light gray fine-grained sand. This is followed by light brown, slightly sandy clay with black smudges at the base (Bed 7) and red sandy clay preserved only in relics (Bed 6). The above lying brown to brown-red clay (Bed 5), massive in the lower portion and containing 1–3 mm thick laminae in the upper portion, is overlain by gray to yellowish sandy clay to clayey medium-grained sand (Bed 4) and brown clay (Bed 3) containing lenses of light brown, medium-grained sand (Bed 2). The section is covered with brown-red clay with sporadic angular clasts of sandstone up to 7 cm in size filling the space formed by water running along the limestone walls.

The NE face of the test-pit shows a similar succession as the opposite SW face of the section (Fig. 4). Minor unconformities and clay fragments are noticeable in the laminated fine-grained sands forming Bed 9 (Fig. 3). Laminated sediments in the left part of the bed were disturbed by a fissure. Small fragments (< 1 mm) of disintegrated darker laminae concentrate along this fissure.

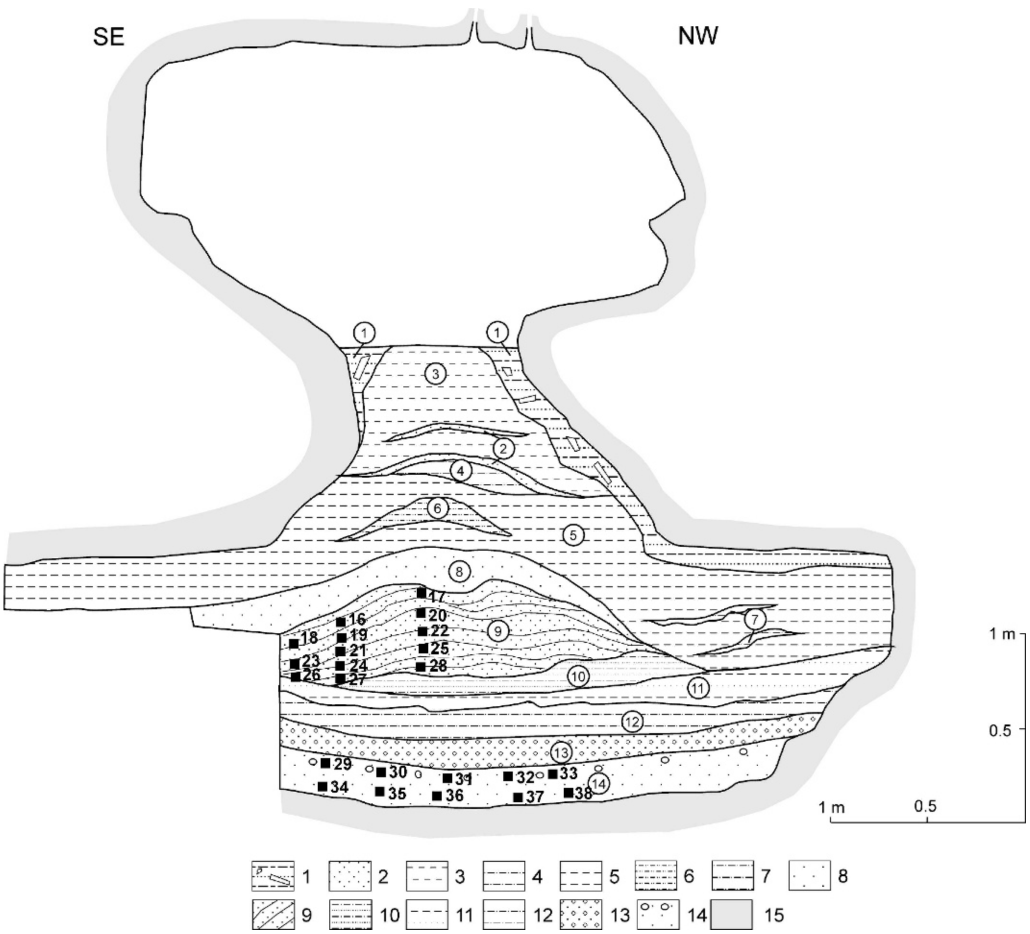

Figure 4. Section 1 — NE face

1 – clay, sporadic angular clasts of sandstone up to 7 cm large; 2 – sand; 3 – clay; 4 – clay; 5 – clay; 6 – sand; 7 – slightly sandy clay; 8 – sand; 9 – sand, fine-grained; 10 – clayey sand, laminated; 11 – clayey sand; 12 – clayey sand; 13 – sand with sandy aggregates; 14 – sand; 15 – bedrock wall; black squares with numbers – collected samples. For more detailed description see text.

SECTION 2

The section is exposed in an older excavated test-pit. Dark brown to gray, medium-grained sand with sporadic clasts of SiO_2-cemented sand up to 1.5 cm in size and rare fragments of brown clay up to 4 cm in size were deposited at the bedrock bottom (Bed 7 in Fig. 5). The above lying gray to yellow brown medium sand with sandy aggregates (Bed 6) contains aggregates of SiO_2-cemented sand up to 1.5 cm in size. Dark gray medium-grained clayey sand layers with lighter stains containing irregular lenses of yellow-brown sand and fragments of brown massive clay up to 1.5 cm in size deposited on the surface of the bed designated as Bed 5. The younger Bed 4 is formed by dark gray, fine-grained silty sand, partly laminated with 1 mm thick laminae of yellow-brown fine sand in the lower portion and lenticular fragments of brown clay indicating erosional surfaces of laminae. The above lying light brown, slightly clayey, medium-grained sand contains relics of cemented sand on its surface (Bed 3). Brown to slightly red laminated clay colored by Mn-oxides in the upper portion represents Bed 2. The top of the succession is formed by light brown to yellow-brown, medium-grained clayey sand containing angular sandstone clasts 5–15 cm in size and fragments of brown and black clay coloured by Mn-oxides (Bed 1). A limestone block up to 0.5 m large is present in the youngest bed.

SECTION 2A

This sedimentary section is exposed in a phreatic conduit about 0.5 m above the top of Section 2. It consists of brown-red, medium-grained sand (Bed 2) and is overlain by light brown clay (Bed 1 in Fig. 5).

SECTION 3

The lowermost Bed 3 of the section is formed by dark gray medium-grained sand beds (1–1.5 cm thick) with brown clayey medium-grained sand and brown clay (0.5–2 cm thick) (Fig. 6). The above lying Bed 2 comprises

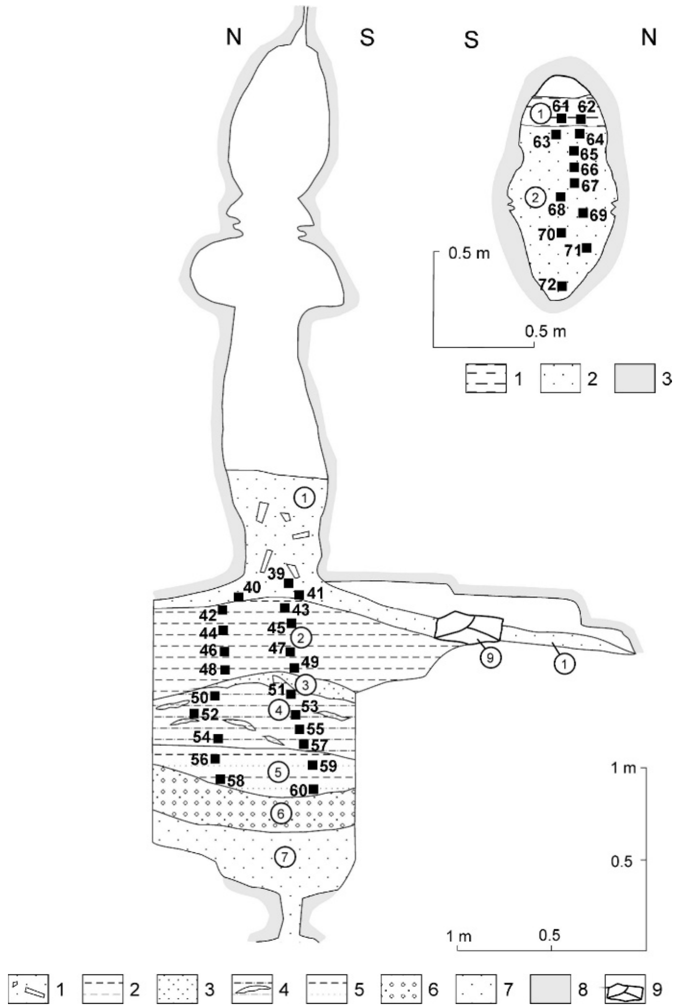

Figure 5. Section 2

1 – clayey sand, rare angular sandstone clasts 5–15 cm large and fragments of clay; 2 – clay, laminated in the upper portion; 3 – slightly clayey sand; 4 – silty sand; 5 – clayey sand; 6 – sand with sandy aggregates; 7 – sand, sporadic sandy concretions up to 1.5 cm large and rare fragments of brown clay up to 4 cm large; 8 – bedrock wall; 9 – block of bedrock; black squares with numbers – collected samples. For more detailed description see text.

Section 2A (top right)

1 – clay; 2 – sand; 3 – bedrock wall.

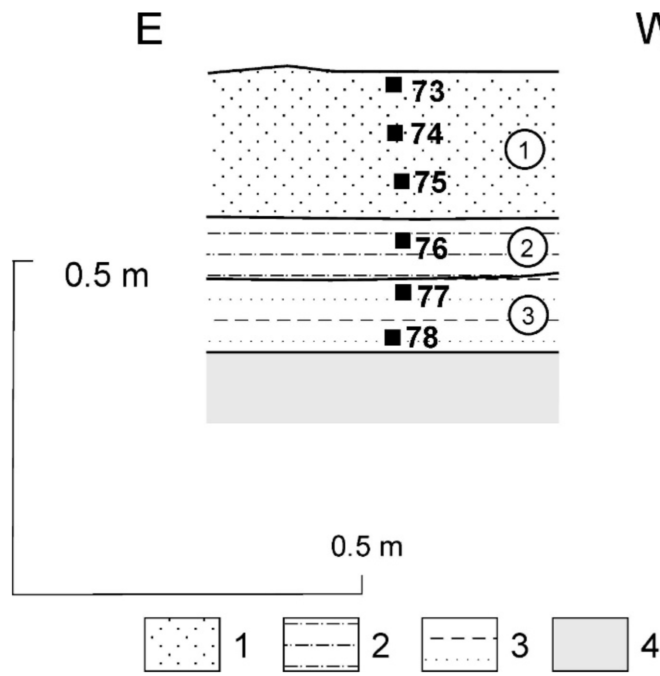

Figure 6. Section 3

1 – sand; 2 – clayey sand; 3 – alternating of layers of sand with clayey sand and clay; 4 – bedrock bottom; black squares with numbers – collected samples.

alternating dark gray laminae of medium-grained clayey sand. The deposition was terminated by a gray to gray-black, medium-grained sand bed with irregular lenses of light brown sand (Bed 1).

Section 4

Yellow-gray, medium-grained sand is exposed in the lowermost Bed 4 (Fig. 7). Light brown, medium-grained sand with gray-brown lenticular stains was deposited in the above lying Bed 3. Bed 2 is formed by dark gray, fine- to medium-grained sand laminae alternating with light brown sand laminae. The section is topped by brown clay alternating with irregular beds of gray, medium-grained clayey sand (Bed 1). A black lamina coloured by Mn-oxides occurs at the base of this bed.

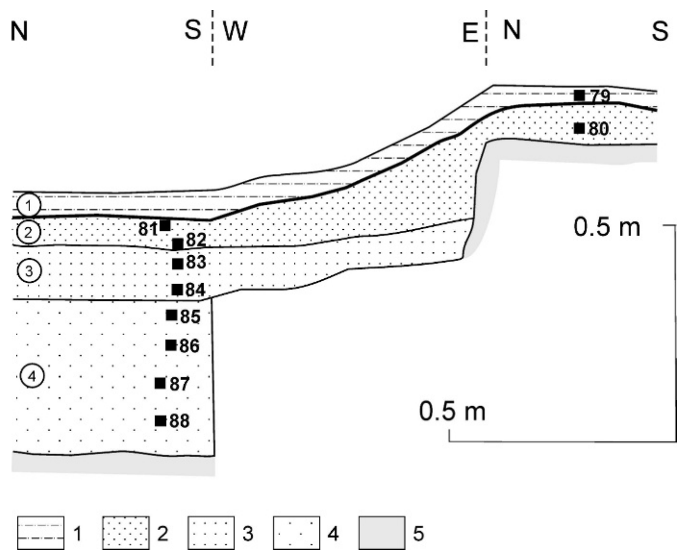

Figure 7. Section 4

1 – clay; 2 – sand; 3 – sand; 4 – sand; 5 – bedrock bottom; black squares with numbers – collected samples.

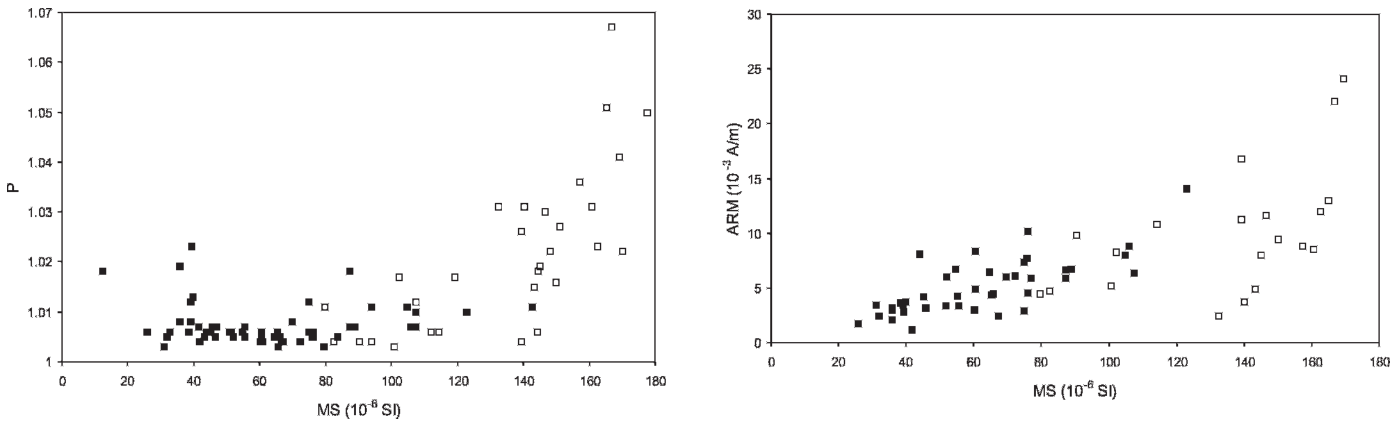

Figure 8. Correlation between magnetic susceptibility (MS) and degree of magnetic anisotropy (*P*) – left; correlation between magnetic susceptibility (MS) and anhysteretic remanent magnetization (ARM) – right. Black squares – bottom sedimentary beds (samples 16–41, 50–60, 63–72, 79–88); empty squares — top sedimentary beds (samples 01–15, 42–49, 61–62, 73–78).

Results

Mineral Magnetic Characteristics and Magnetic Fabric

The MS values slightly increase from sandy bottom sediment beds to the above lying clay dominating sediments (Fig. 8). In Section 1, the values range from 23–63 × 10^{-6} SI (Bed 14) to 30–119 × 10^{-6} SI (Bed 9) and 90–149 × 10^{-6} SI (Beds 3 and 5). Similar variations were measured in Section 2 with 37–73 × 10^{-6} SI (Beds 4 and 5), 67–127 × 10^{-6} SI (Bed 2) and 56–90 × 10^{-6} SI (Bed 1). Basal sands in Section 2A yielded MS values of 22–55 × 10^{-6} SI (Bed 2), whereas the above lying clay bed has MS values of 121–123 × 10^{-6} SI (Bed 1). MS values of sediments exposed in Section 3 range between 76 and 124 × 10^{-6} SI, whereas the values in Section 4 slightly increase from 10–35 × 10^{-6} SI (in beds 3 and 4) to 26–94 × 10^{-6} SI (Bed 2). The highest MS values (up to 410 × 10^{-6} SI) were measured in the modern topsoil collected above the Medeo Entrance, whereas the bedrock sandstone showed MS values between 7 and 25 × 10^{-6} SI and MS values of limestone are about 10 × 10^{-6} SI. The ARM values ranging between 1 and 22 × 10^{-3} A/m plot versus the MS show steep increase in the top beds (Fig. 8). The AMS degree also increases in these beds (Fig. 9). The magnetic fabric of the sediments is mostly oblate. Basal sands in sections 1, 2 and 4 show more prolate fabric as expressed by negative *T* values (Fig. 9).

The magnetic lineation directions in the top sedimentary beds show concentration in NW to SW directions (Fig. 10, top left) with the mean direction tending to the WSW. The poles to magnetic foliation are usually concentrated around the center of the projection. N-S elongation of the pole directions was found in sediments from Section 3 (Fig. 10, top right). The magnetic lineation directions measured in the bottom sedimentary beds show almost random distribution accompanied by large dispersion of poles to magnetic foliation (Fig. 10, bottom).

Exoscopy of Quartz Grains

Three types of microstructures were observed on quartz grain surfaces: (i) precipitation of SiO_2 on the surface of grains in lace-like patterns, (ii) corrosive etched microstructures, and (iii) overgrowth with quartz crystals. The bedrock Ordovician sandstone forming the ceiling of the cave passage above Section 2 contains rounded quartz grains about 1 mm in diameter (Fig. 11, top left). The grain surfaces show weak dissolution and precipitation of SiO_2 (Fig. 12, bottom left). The cross-bedded sandstone forming intercalations in the limestone contains smaller quartz grains cemented with SiO_2 into aggregates with an average length of 1 mm (Fig. 11, top right). The basal sand in Section 1 consists of separate rounded grains with average size of about 0.5 mm (Fig. 11, bottom left). Surfaces of many grains are modified by conchoidal fractures and corrosion features. Grain aggregates with weakly corroded

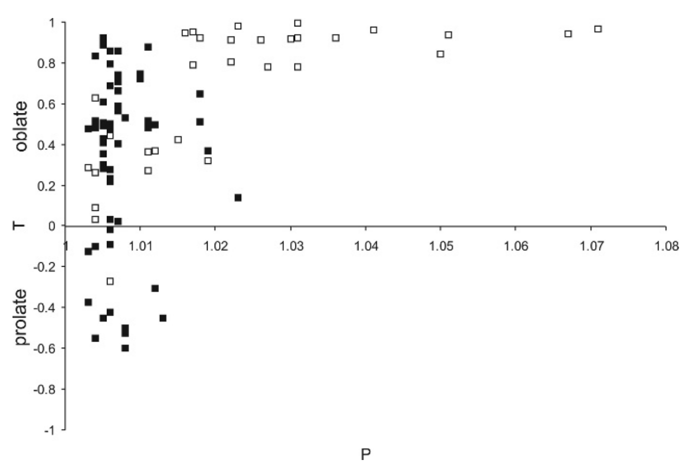

Figure 9. Correlation between degree of anisotropy (*P*) and shape of anisotropy ellipsoids (*T*). Sample symbols are the same as in Fig. 8.

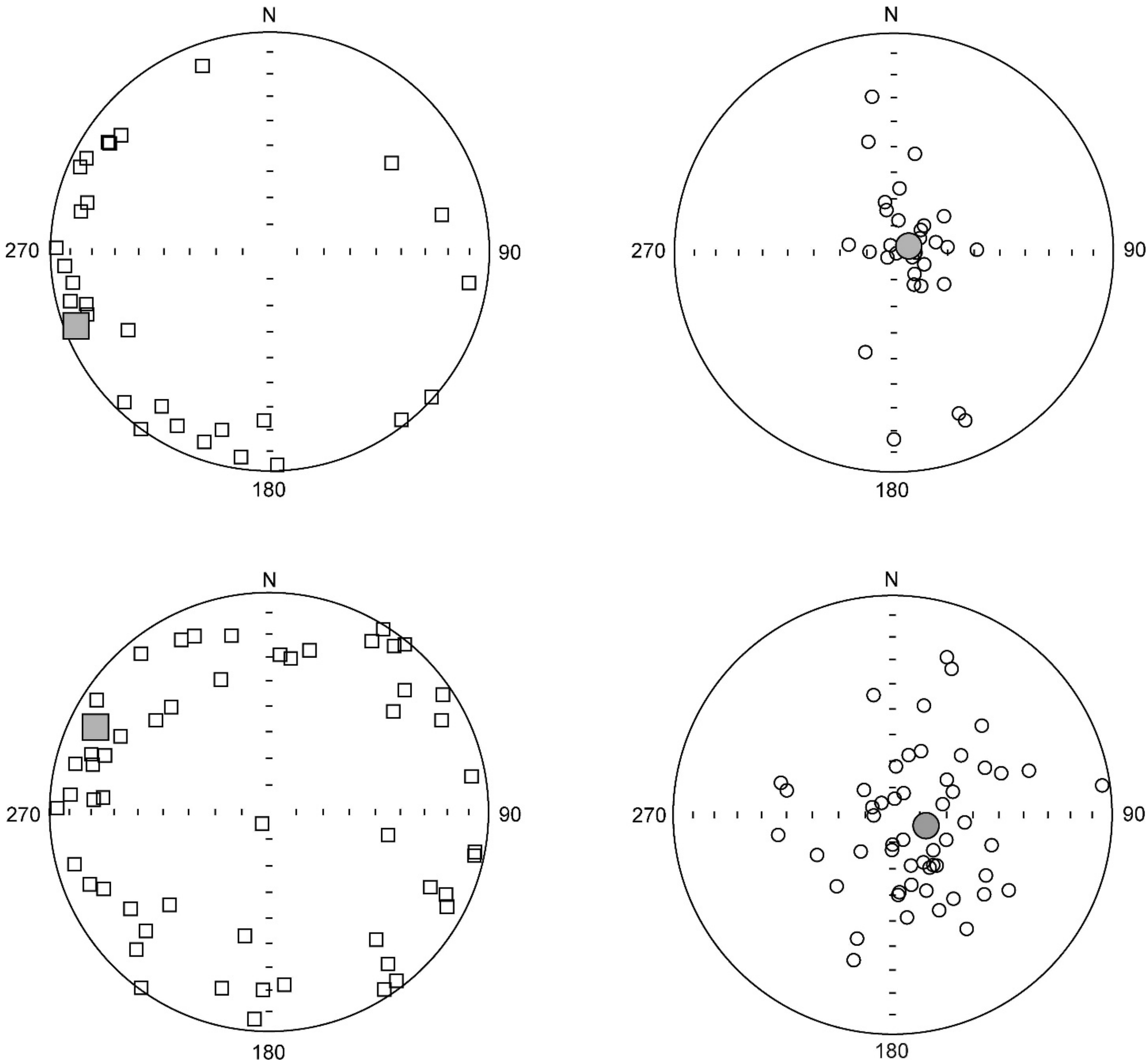

Figure 10. Principal directions of magnetic fabric of sediments indicated by anisotropy of magnetic susceptibility; equal-area projection on the lower hemishere. Top left – magnetic lineation in bottom sedimentary beds; top right – pole to magnetic foliation in bottom sedimentary beds; bottom left – magnetic lineation in top sedimentary beds; bottom right – poles to magnetic foliation in bottom sedimentary beds; larger gray squares and circles represents mean directions.

surfaces dominate in the above lying Bed 9 (Fig. 11, bottom right). Angular flat mineral particles (micas?) dominate in Bed 3, separate quartz grains and aggregates are present in smaller amounts (Fig. 12, top left). Quartz grains in sand deposited in the bottom beds in Section 2 (Beds 6 and 7 in Fig. 5) form cemented aggregates up to 1 mm large as in the bottom beds of Section 1. Grain surfaces often bear lace-like silica coatings. The above lying Bed 4 in Section 2 is composed of a mixture of free grains (30 %) and cemented aggregates (70 %) with lace-like silica coatings. Angular mineral particles are rarely present in the bed. Sub-angular to rounded grains up to 1 mm in size prevail in Bed 1 against cemented grain aggregates showing weak roundness. Sand from Bed 2 in Section 2A shows predominantly free rounded quartz grains coated with lace-like silica (Fig. 12, bottom right). Exoscopic analyses were completed with images from modern soil collected at the Medeo Cave entrance. Free rounded quartz grains up to 1.5 mm in size dominate in the soil (Fig. 12, top right).

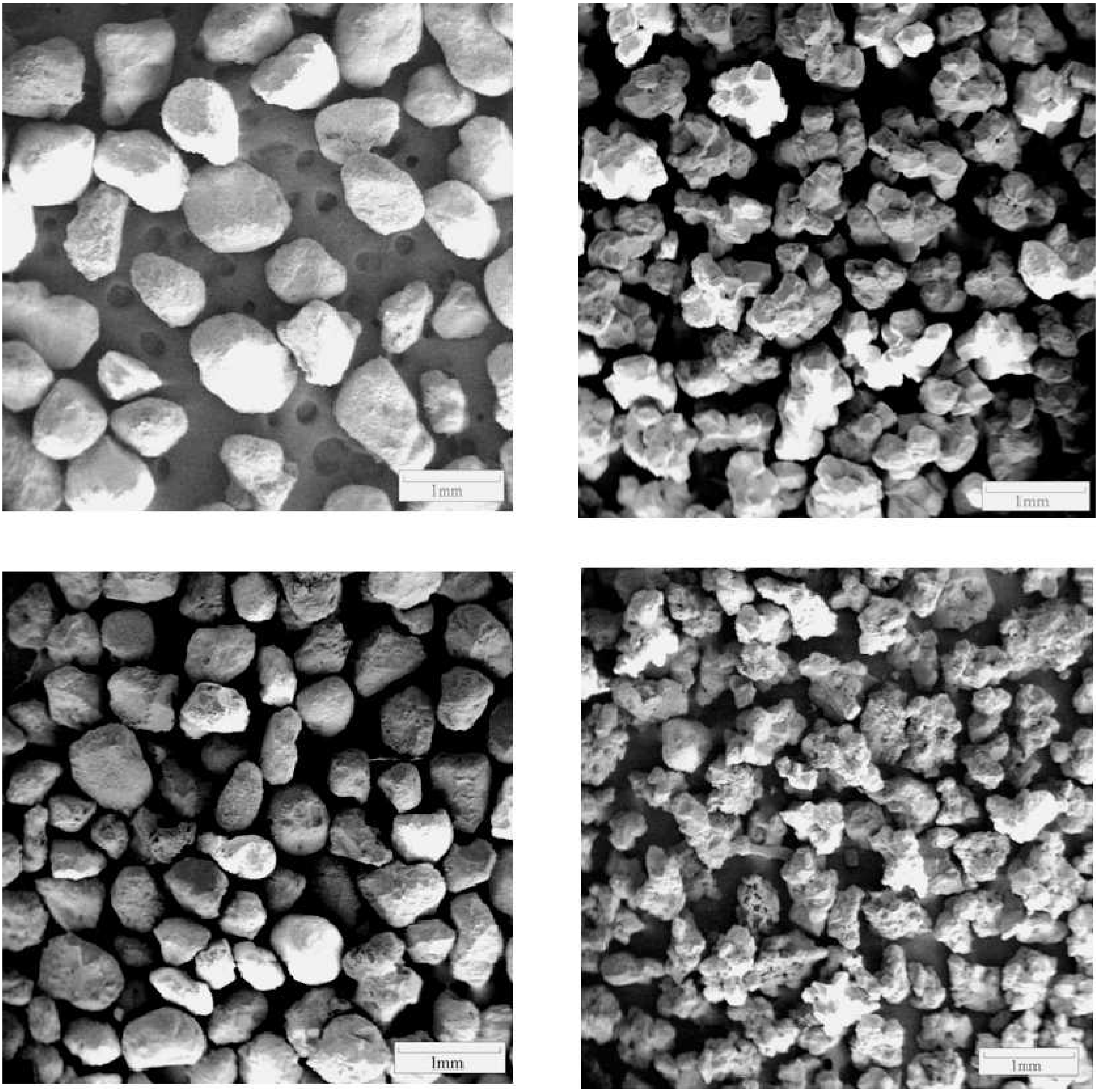

Figure 11. Surface of quartz grains. Top left – quartz from bedrock sandstone; top right – quartz aggregates from cross-bedded sandstone intercalated within the limestone; bottom left – quartz from Bed 15 in Section 1; bottom right – quartz aggregates from Bed 9 in Section 1.

The quartz grain aggregates isolated from Bed 14 in Section 1 were put through an experiment using a kitchen blender simulating transport of sediments in a turbulent flow. The aggregates were almost completely disintegrated after 5 minutes of mixing. The silica coatings on grain surfaces were destroyed after 15 and 30 minutes of mixing.

HEAVY MINERAL CONTENT

The studied samples of the bedrock and cave deposits show monotonous association of stable heavy minerals. Grains of transparent heavy minerals are rounded, while the opaque mineral grains are mostly angular. Beds in the upper portions of Sections 1 and 2 contain greater amounts of garnet, similar to modern soil (Table 1).

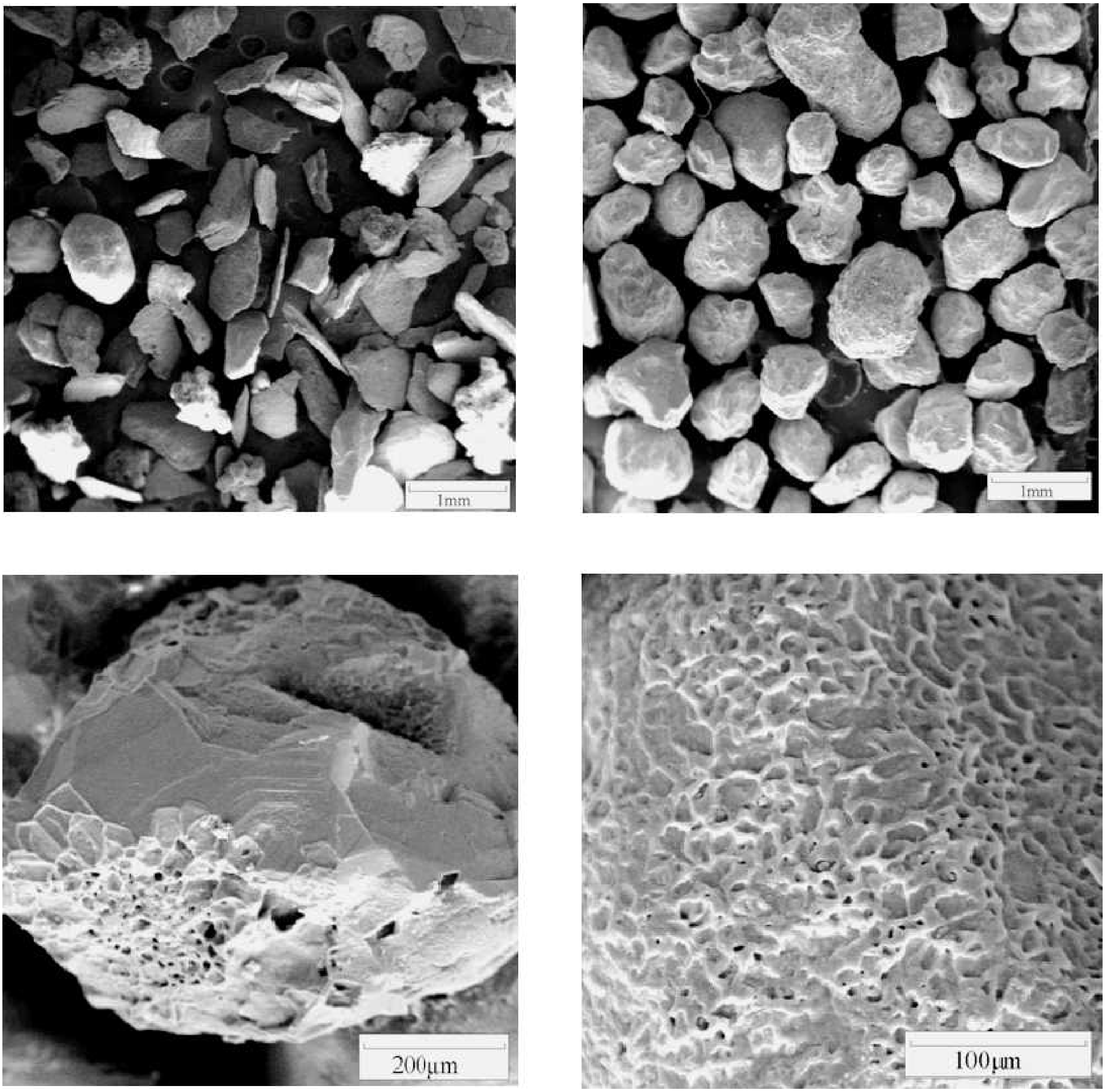

Figure 12. Surface of quartz grains. Top left – mixture of quartz and angular grains from Bed 3 in Section 1; top right – quartz from modern soil; bottom left – a detail of quartz corrosion from Bed 15 in Section 1; bottom right – a detail of newly-formed quartz precipitates from Bed 2 in Section 2A.

These deposits reveal an opaque/non-opaque mineral ratio 1:3 while other sediments studied contain a higher proportion of opaque minerals. Higher concentrations of garnet were also determined in the basal sand from Bed 14 in Section 1. Staurolite dominates in sediments with lower garnet content, including the bedrock sandstone (Table 1).

Flowstone Dating

Radiometric dating of the flowstone bed by $^{230}Th/^{234}U$ method reveals that the age of three dated samples exceeds 350 ka (limit of the dating method). However, the flowstone age higher than 1.2 Ma cannot be eliminated based on $^{234}U/^{238}U$ ratio (Table 2). During thermal demagnetization experiments magnetic moment decreased

Table 1. Heavy mineral content in modern soil, cave deposits and bedrock (values are in percent).

Cave Deposit	Garnet	Staurolite	Zircon	Rutile	Opaque/Non-Opaque Mineral Ratio
Modern Soil	72	24	2	3	1:3
Section 1 – Bed 3	80	5	15	1	1:3
Section 1 – Bed 9	4	89	5	2	1:1
Section 1 – Bed 14	3	85	7	5	1:1
Section 1 – Bed 15	45	49	3	3	8:1
Section 2 – Bed 1	35	56	2	8	1:1
Section 2 – Bed 4	7	82	9	2	1:1
Section 2 – Bed 6	9	80	7	4	1:1
Section 2A – Bed 2	50	36	10	4	1:3
Ordovician Sandstone	4	86	5	5	1:1

with increasing temperatures (Fig. 13, bottom). Directional variations of magnetic vector during the demagnetization process are expressed in the Zijderveld diagram and in the stereographic plot (Fig. 13, top). The mean paleomagnetic direction is: Declination = 18°, Inclination = 61°. Based on these paleomagnetic data, it is evident that the flowstone records normal polarity of the Earth magnetic field from the time of the carbonate deposition.

Discussion of Results

Based on obtained results the sedimentary beds exposed in the studied sections were subdivided in two parts with the bottom (older) beds (beds 9–14 in Section 1, beds 4–7 in Section 2, Bed 2 in Section 2A and beds 2–4 in Section 4) and top (younger) beds (beds 1–8 in Section 1, Bed 1–3 in Section 2, Bed 1 in Section 2A, beds 1–3 in Section 3 and Bed 1 in Section 4).

The bottom beds reveal similar lithological, magnetic and heavy metal properties (except of sand in Bed 14). Basal sand deposited on the bedrock bottom shows a lower MS, similar to the bedrock sandstone. The exoscopic quartz grain characteristics are similar, too. It can therefore be proposed that the deposits filling the bottom part of cave corridors were derived from the local bedrock formed by Early Ordovician sandstones. The good roundness of quartz grains is a result of grain reworking in a high-energy Ordovician marine environment. Later, long distance redeposition of these quartz grains by Cenozoic streams can be excluded by the results of liquidizer experiment testing of the resistance of quartz grain aggregates during turbulent fluvial transport. No source of larger SiO_2-cemented aggregates (max. 2 cm long) common in beds 13 and 14 in Section 1 was found. These aggregates were cemented *in situ* during different climatic conditions allowing SiO_2 dissolution and precipitation. Sands in beds 11–13 in Section 1 and in Beds 6 and 7 in Section 2 lack prominent lamination or cross bedding (unlike the overlying sediments). It can be therefore assumed that these beds also belong to the bottom fill of cave passages.

The younger cross-bedded and laminated, mostly clayey sands in beds 8–10 (Section 1) and beds 3 and 4 (Section 2) were deposited after partial erosion of the basal deposits. The deposits reveal slightly higher MS values. The exoscopic observation shows cemented quartz grain aggregates indicating the source in the local cross-bedded sandstone (comp. Fig. 11, top right and Fig. 11, bottom right). The inner structures of these laminated sediments (small unconformities, redeposited fragments of clay, laminae partly cemented by carbonate and erosional surface of Bed 10) show a frequent alternation between local aggradation and erosion events. The sediments were deposited during heavy precipitation events, when water penetrated into the cave corridors from the surface through the swallow holes and along open cracks. The water escape structures (e.g., the fissure in beds 9–11, Section 1) were formed during the compaction of sediments. Sand grains accumulating along the fissures were later partly cemented by carbonate. Pore fluids moved during repeated liquefaction of the sediments and disturbed the primary magnetic fabric of these deposits, resulting in the tilting of the magnetic foliation to the NW (Fig. 10, bottom right). However, it is not possible to determine the flow direction

Table 2. Th/U age of the flowstone relic.

Sample Name	Sample Lab. No.	U (ppm)	$^{234}U/^{238}U$	$^{230}Th/^{234}U$	$^{230}Th/^{232}Th$	Age (ka)
BT 2	W 1302	28.2 ± 0.7	1.005 ± 0.005	1.064 ± 0.005	> 1000	> 350
BT 3	W 1301	19.8 ± 0.7	1.002 ± 0.007	1.002 ± 0.007	450 ± 40	> 350
BT 6	W 1303	11.9 ± 0.4	1.009 ± 0.008	1.083 ± 0.008	520 ± 60	> 350

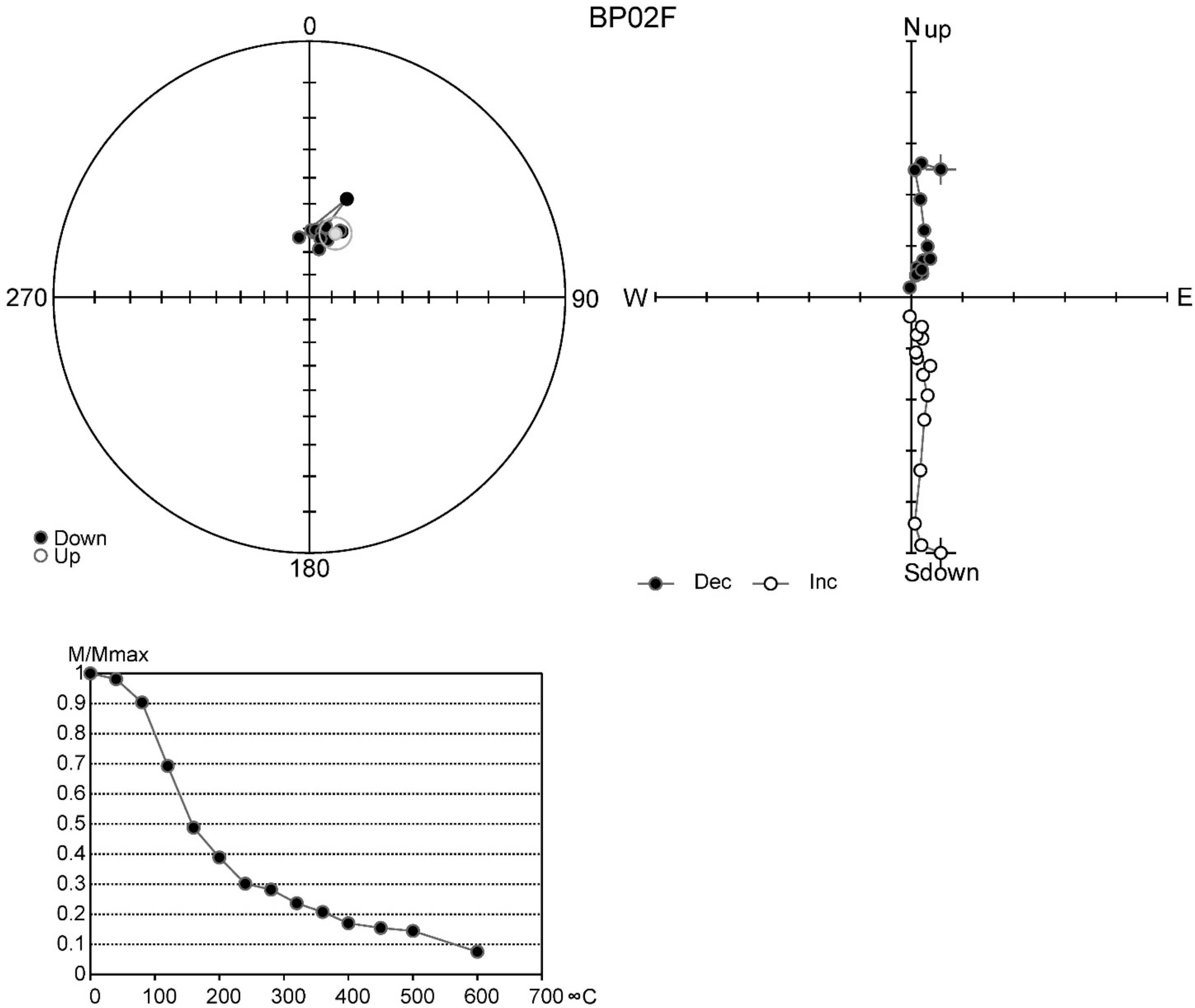

Figure 13. Thermal demagnetization of the flowstone sample BP02F. Top left – directions of magnetization vector during demagnetization process, black circles – projection of vector directions to the lower hemisphere, gray point in the circle – interpreted direction of the primary component of the magnetization vector; top right – Zijderveld diagram, black circles – projection of vector directions into horizontal plane, white circles – projection of vector directions into vertical plane; bottom left – normalized magnetization intensity values during the thermal demagnetization.

due to random dispersion of magnetic lineation directions measured in the bottom bed sediments.

Clayey sands forming the top portions of Section 1 (Beds 2–7) and Section 2 (Bed 2) reveal still higher MS values and higher garnet content, similar to the modern soil from the surface above the cave. The magnetic lineation and foliation indicate a calmer sedimentary environment with slow sediment transport directions from NW, W and SW (Fig. 10, top). Elongation of k_3 orientations in N-S direction measured in Section 3 could be a result of post-depositional deformation of the cave sediments caused by frost when the sedimentary layers filling narrow cave passage could be deflected due to volume changes. In the cave sediments with higher clay content, the MS increases together with the degree of anisotropy (Fig. 8, left). Different heavy mineral content of the sediments, compared to the bottom portions of the sections, indicates a different source of these deposits. The sediments could have been originally transported by wind to the area of Botovskaya Cave, from where they were vertically transported by precipitation waters through swallow holes and along open cracks to the cave. This assumption could be supported indirectly because angular flat mineral particles are missing in bottom cave sediments. Higher MS values of the clayey sediments correspond with the high MS of the topsoil at the cave surface. Most part of the iron present in the modern soil is the paramagnetic Fe^{3+} form (almost 80 %, identified by Mössbauer spectroscopy), which may be the result of weathering of paramagnetic minerals during pedogenic processes (e.g., Evans and Heller, 2004). The presence of superparamagnetic (SP) minerals originating during pedogenesis or taiga forest fires cannot be excluded (Thompson and Oldfield, 1986). However, results of frequency dependent magnetic susceptibility measurements, usually supporting SP mineral presence (e.g., Dearing, 1999), are not very reliable due to low MS values of the cave sediments.

MS of sand filling the karst conduit with Section 2A (Bed 2) is similarly low as in the basal sands in Section 2. Nevertheless, it differs from the latter in the high proportion of garnet (much like in Bed 14 in Section 1). The overlying clay in this section has similar properties to the youngest deposits in Sections 1 and 2 and the modern soil. However, precipitation waters flowing vertically from the surface through open fissures also transported the clay. Heavy precipitation events resulted in the erosion of the top part of the sediment in both Sections 1 and 2 and resulted in the deposition of clay-dominated sediments with chaotically arranged angular clasts of sandstones and with limestone blocks (Bed 1 in both sections).

Taiga forest fires could control the mechanism of sediment transportation from the surface above the cave to the underground passages. The topsoil retention ability is usually dramatically decreased after forest fires due to damaged vegetation. Precipitation would then percolate very fast into the cave. Evidence of a past catastrophic erosion event is preserved about 50 m west of Section 1 (Fig 2). A relic of flowstone bed is preserved on the limestone wall 1.7 m above present passage floor. The flowstone bed was originally deposited on the top of the clastic deposits, which filled the passage. The radiometric and paleomagnetic polarity dating suggests a likely age for the carbonate bed between 350 and 780 ka (i.e., older than $^{230}Th/^{234}U$ method age limit and but still within the present normal-polarity Brunhes Chron). However, we cannot entirely exclude the flowstone deposition during any older normal-polarity periods. In such case the flowstone should be older than 2.58 Ma (i.e., Matuyama-Gauss paleomagnetic boundary). We do not suppose a speleothem deposition during relatively short normal-polarity Jaramillo or Olduvai subchrons. Anyway, in the time of the flowstone deposition the artesian aquifer regime was already disrupted due to surrounding valley incision and vadose conditions dominated in the cave system. The later intensive erosion removed clastic sediments from under the flowstone bed and destroyed the entire flowstone. This erosional event had to be triggered by unusually heavy precipitation, which entered the bedrock through vertical ruptures opened both in sandstone and limestone due to differential subsidence of the massif (see below). The surrounding valleys supporting this vertical movement should be developed. Therefore, we suppose that the erosion occurred most probably during the Middle or Late Pleistocene. At that time the local surface streams were incised at a much lower position than the Botovskaya Cave. Results of this catastrophic cave flood could be the chaotic sediments deposited in Bed 1 in the Sections 1 and 2.

The morphology of the cave passages documents transverse flow under confined hydrological conditions in the artesian aquifer connected with upward solution of limestone (Klimchouk, 2000, 2003; Filippov, 2000). In the subsequent period lower parts of the passages were widened to the shape of a relatively broad channel with a flat ceiling. It should indicate a long-term dissolution, when the passages were permanently flooded with stagnant water. It is not easy to reconstruct this period in the cave system development, because this channel is completely filled with clastic cave deposits and is noticeable only in the excavated test-pits. We assume a period of relative stability and propose that the cave system was lying near the level of the ground-water table prior to the incision of the present deep valleys (Lena River) in the vicinity of the cave system. This stage should be dated to the Miocene, because the cave is located above the Pliocene river terrace level (Filippov, 2000).

Structures preserved in the clastic sediments filling the cave passages indicate deposition mostly in vadose conditions with frequent alternations of deposition and erosion. The water escape structures detected in sediments similar to silty laminae cemented by carbonate (Bed 9 in Fig. 3) support our assumption that the clastic deposition occurred in cave passages, which were not completely filled with water.

The following incision of surrounding valleys was probably triggered by a substantial Late Pliocene uplift recorded in the Lake Baikal Cenozoic sediments (Mats et al., 2000). Stability of the sedimentary massif comprising the Botovskaya Cave deteriorated as a result of this Pliocene-Pleistocene incision.

This was accompanied by gravity-induced opening of N–S joints parallel to the slope of the Garevogo Creek, where cave entrances are located, and by NE–SW opened joints parallel to the Lake Baikal rift structure indicating ongoing uplift connected with extension of the area (cf., Zorin et al., 2003). These ruptures detected at many places in the Old World of the Botovskaya Cave are now used by water seeping from the surface above the cave. These vertical pathways are also used for the underground transport of clastic sand- and clay-dominated sediments from the surface above the cave. Such a place is located east of Section 1. Sandstone blocks fallen from the ceiling are covered by light brown sands and clays (much like in Section 2A). Relicts of clayey sand are also preserved in hanging positions on rock ledges above the test-pit with Section 1. These clastic sediments do not, however, cover blocks pertaining to a younger phase of ceiling destruction. It is probable that the last falling of ceiling slabs also took place recently. Erosion caused by flowing water results, in turn, in further stability deterioration of the sandstones under- and overlying the limestone bed. Such weak points in the cave system then experience large collapse of the sandstone slabs from the ceiling and formation of chokes. Intensive water flow is also responsible for the growth of flowstone decorations at such places.

Conclusions

Three specific conclusions can be drawn from this study. First, the sections in detrital cave sediments in Botovskaya Cave (in The Old World part) evidence periodical sediment deposition. It cannot be excluded that the individual beds are separated by long hiatuses. Sediments of the cave fill are of two different types: the older, bottom sands are derived from weathered bedrock sandstones and were probably horizontally transported over a short distance. The overlying sediments dominated by clay and clay/sand were transported vertically with precipitation waters from the surface above the cave. The contrasting mineralogical and magnetic parameters of these top sediments indicate a different (more distant?) source.

Second, if the bottom sand was transported horizontally through the cave by flowing water, it must have taken place before the incision of the present deep valleys, probably in the Late Tertiary. Finer sediments should be transported by wind and deposited on the surface above the cave. From there, they were removed by precipitation waters together with weathered surface products and deposited in cave passages. These processes, most probably of Quaternary age, were lacking any direct link to the local hydrologic network.

Third, morphologies of passages in Botovskaya Cave document two stages of the cave system development: the older, characterized by confined hydrological conditions in the artesian aquifer. Passages formed during this older stage were later partly remodeled by stagnating water corrosion. This younger stage affected the cave system probably in the Tertiary, before the deep river valleys were formed.

Acknowledgements

The project was supported by the INTAS Program No. 03-51-4152: Speleothems and other cave sediments from Siberia: an archive from the boreal climate zone with the potential for climate reconstruction on an annual to decadal basis (SPELEOARCH) and it is a part the research project of the Institute of Geology AS CR, v.v.i. No. AV0Z30130516.

References

Breitenbach, S., 2004, High-resolution isotope measurements ($\delta^{18}O$ and $\delta^{13}C$) from Siberian stalagmites as potential palaeoclimatic proxies [MSc. thesis], Humboldt Universität, 72 p.

Dearing, J., 1999, Magnetic susceptibility, *in* Walden, J., Oldfield, F., and Smith, J., eds., Environmental magnetism: A practical guide, Quaternary Research Association, Technical Guide No.6, p. 35–62.

Ellwood, B.B., Petruso, K.M., Harrold, F.B., and Korkuti, M., 1996, Paleoclimate Characterization and Intra-Site Correlation Using Magnetic Susceptibility Measurements: An Example from Konispol Cave, Albania: Journal of Field Archaeology, v. 23, p. 263–271.

Ellwood, B.B., Harrold, F.B., and Benoist, S.L., 2004, Magnetic susceptibility applied as an age-depth-climate relative dating technique using sediments from Scladina Cave, a Late Pleistocene cave site in Belgium: Journal of Archaelogical Science, v. 31, no. 3, p. 283–293.

Evans, M.E., and Heller, F., 2004, Environmental Magnetism: Principles and Applications of Enviromagnetics, San Diego, Academic Press, 299 p.

Filippov, A.G., 2000, Speleogenesis of Botovskaya Cave, Eastern Siberia, Russia, *in* Klimchouk, A.B., Ford, D.C., Palmer, A.N., and Dreybrodt, W., eds., Speleogenesis, Evolution of Karst Aquifers, Huntsville, Ala., National Speleological Society, p. 282–286.

Göbel, E., and Breitenbach, S., 2003, Die Peschera Botovskaja, die längste Höhle Russlands: Mitteilungen des Verbandes der Deutschen Höhlen - und Karstforscher, v. 49, no. 2, p. 42–45.

Gorka, P., and Hercman, H., 2002, URANOTHOR v. 2.5., Delphi Code of calculation program and user guide: MS, Archive of Quaternary Geology Department, Institute of Geological Sciences, PAS, Warsaw, 65 p.

Häuselmann, P., Granger, D.E., Lauritzen, S.E., and Jeannin, P.Y., 2007, Abrupt glacial valley incision at 0.8 Ma dated from cave deposits in Switzerland: Geology, v. 35, no. 2, p. 143–146.

Ivanovich, M., and Harmon, R.S., 1992, Uranium Series Disequilibrium: Applications to Environmental Problems, Oxford, Clarendon Press, 2nd edition, 910 p.

Jelínek, V., 1981, Characterization of the magnetic fabric of rocks Tectonophysics, v. 79, T63–T67

Kadlec, J., Hercman, H., Beneš, V., Šroubek, P., Diehl, J.F., and Granger, D., 2001, Cenozoic history of the Moravian Karst (northern segment): Cave sediments and karst morphology: Acta Musei Moraviae, Scientiae Geologiae, v. 85, p. 111–161.

Klimchouk, A., 2000, Speleogenesis under deep-seated and confined settings, *in* Klimchouk, A.B., Ford, D.C., Palmer, A.N., and Dreybrodt, W., eds., Speleogenesis, Evolution of Karst Aquifers, Huntsville, Ala., National Speleological Society, p. 244–260.

Klimchouk, A., 2003, Conceptualisation of speleogenesis in multi-storey artesian systems: a model of transverse speleogenesis, http://www.speleogenesis.info/archive/publication.php?PubID=24&Type=publication&keyword=Klimchouk

Mats, V.D., Khlystov, O.M., De Batist, M., Ceramicola, S., Lomonosova, T.K., and Klimansky, K., 2000, Evolution of the Academician Ridge Accommodation Zone in the central part of the Baikal Rift, from high-resolution reflection seismic profiling and geological field investigations: International Journal of Earth Science, v. 89, p. 229–250.

Nagata, T., 1961, Rock Magnetitism, Tokyo, Maruzen, 2nd edition, 350 p.

Sroubek, P., Diehl, J.F., Kadlec, J., and Valoch, K., 2001, A Late Pleistocene paleoclimatic reconstruction based on mineral magnetic properties of the entrance facies sediments of Kulna Cave, Czech Republic: Geophysical Journal International, v. 147, no. 2, p. 247–262.

Sroubek, P., Diehl, J.F., and Kadlec, J., 2007, Historical climatic record from flood sediments deposited in the interior of Spirálka Cave, Czech Republic: Palaeogeography, Palaeoclimatology, Palaeoecology, v. 251, p. 547–562.

Thompson, R., and Oldfield, F., eds., 1986, Environmental Magnetism, Allen and Unwin, London, 227 p.

Zorin, Y.A., Turutanova, E.Kh., Mordvinovaa, V.V., Kozhevnikova, V.M., Yanovskayab, T.B., and Treussovc, A.V., 2003, The Baikal rift zone: the effect of mantle plumes on older structure: Tectonophysics, v. 371, p. 153–173.